ACS APPLIED MATERIALS & INTERFACES

Research Article

www.acsami.org

Nonthermal Plasma Synthesis of Core/Shell Quantum Dots: Strained Ge/Si Nanocrystals

Katharine I. Hunter,*[,†] Jacob T. Held,[‡] K. Andre Mkhoyan,[‡] and Uwe R. Kortshagen*[,†]

[†]Department of Mechanical Engineering and [‡]Department of Chemical Engineering and Materials Science, University of Minnesota, Minneapolis, Minnesota 55455, United States

Supporting Information

ABSTRACT: In this work, we present an all-gas-phase approach for the synthesis of quantum-confined core/shell nanocrystals (NCs) as a promising alternative to traditional solution-based methods. Spherical quantum dots (QDs) are grown using a single-stage flow-through nonthermal plasma, yielding monodisperse NCs, with a concentric core/shell structure confirmed by electron microscopy. The in-flight negative charging of the NCs by plasma electrons keeps the NC cores separated during shell growth. The success of this gas-phase approach is demonstrated here through the study of Ge/Si core/shell QDs. We find that the epitaxial growth of a Si shell on the Ge QD core compressively strains the Ge lattice and affords the ability to manipulate the Ge band structure by modulation of the core and shell dimensions. This all-gas-phase approach to core/shell QD synthesis offers an effective method to produce high-quality heterostructured NCs with control over the core and shell dimensions.

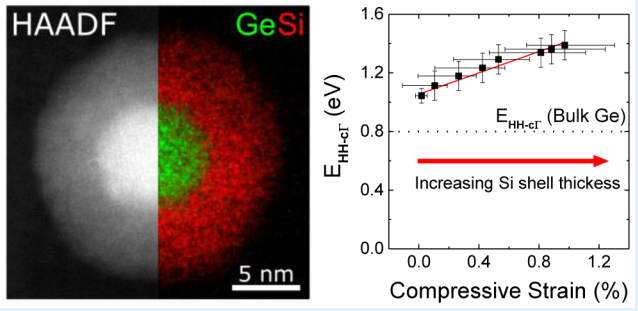

KEYWORDS: *silicon, germanium, core/shell nanocrystal, nonthermal plasma, strained epitaxy, heterostructure*

INTRODUCTION

Semiconducting quantum dots (QDs) have drawn increasing interest over the last few decades because of their size-dependent band gaps, providing fine control over their optoelectronic properties.[1] A key advance in colloidal QD engineering has been the development of methods for epitaxial shell growth in solution,[2] notably successive ionic layer adsorption and reaction,[3] which allows for monolayer control over shell growth. These colloidally synthesized core/shell QDs have demonstrated that QD heterostructures provide a powerful means of manipulating material properties through band alignment (type I,[2] type II,[4] quantum well,[5] etc.) and strain.[6]

In this work, we present an all-gas-phase alternative to traditional solution-based approaches for the bottom-up growth of core/shell QDs, tailored toward the incorporation of group IV semiconductors in heterostructured QD systems. The method described in this work has distinct advantages over conventional solution-phase shell-growth techniques. Specifically, it is suitable for materials that require high synthesis temperatures, does not require the addition of electrically insulating ligands, and would allow for the deliberate doping of QD core and/or shell[7] while minimizing chemical waste. The method presented here is broadly applicable for the gas-phase synthesis of many core/shell structures yet unrealized through conventional wet chemistry approaches. In this work, we have investigated the synthesis and optical properties of Ge/Si core/shell QDs with varying shell thicknesses.

Despite the technological importance of bulk group IV semiconductors (Si and Ge), the development of core/shell QDs utilizing these materials has lagged, likely because of the high crystallization temperatures of these materials often requiring high-temperature, gas-phase synthesis.[8,9] In recent years, the use of nonthermal plasmas to synthesize group VI QDs has presented significant advantages over other aerosol-based approaches, resulting in highly crystalline, monodisperse 2−10 nm particles, with tunable absorption and emission.[10] However, the colloidal stability conferred by subsequent organic functionalization results in strong covalent bonds, often rendering these plasma-synthesized group IV QDs incompatible with common solution-phase shell-growth approaches.

According to density functional theory calculations[11] and tight-binding models,[12] the Ge/Si heterostructured QDs investigated in this work are expected to exhibit type II carrier confinement, with holes confined to the Ge core and electrons localized in the Si near the core/shell interface, because of the large valence band offset between Ge and Si. Extensive work on Ge/Si nanowires (NWs) has leveraged the 1D hole gas resulting from this type II alignment to investigate single Ge/Si NW field-effect transistors,[13] Ge/Si NW Josephson Junctions,[14] and Ge/Si NW qubits.[15] Additionally, surface-grown Si-capped

Received: December 18, 2016
Accepted: February 7, 2017
Published: February 7, 2017

DOI: 10.1021/acsami.6b16170
ACS Appl. Mater. Interfaces 2017, 9, 8263−8270

Ge QDs have been investigated for improved metal oxide semiconductor field-effect transistor (MOSFET) memory structures,[16] photovoltaic devices,[17] and thermoelectrics.[18] Importantly, for these Ge/Si nanostructures, the outer Si layer provides a protective barrier against the formation of an inferior Ge oxide and may also be chemically passivated to prevent oxide formation entirely.[19]

Early efforts were made to synthesize Ge/Si nanocrystals (NCs) in solution from Zintl salts.[20] Recent efforts in the aerosol community to produce free-standing Ge/Si NCs have resulted in large 80−100 nm core/shell NCs, beyond the scale of quantum confinement.[21] These particular NCs suffer from a high density of defects in Si the shell and heavy twinning of the Ge core and exhibit large, uncontrolled variation in the shell thickness. The shortcomings of this neutral aerosol method provide significant evidence for the importance and success of our nonthermal plasma approach, particularly in terms of control over the size and morphology.

EXPERIMENTAL DETAILS

In this work, Ge/Si core/shell QDs with increasing Si shell thickness were synthesized using the nonthermal plasma reactor diagrammed in Figure 1a. This simple flow-through design was adapted from Mangolini et al.[10] for the nonthermal plasma synthesis of group IV QDs but modified to include a secondary gas stream for epitaxial shell growth.

Ge Core Growth. Ge NC cores are grown in the bulk of the plasma, as described elsewhere.[24] In short, the primary gas feed—a mixture of argon (Ar), hydrogen (H_2), and germanium tetrachloride ($GeCl_4$) vapor—enters through the top of the 1-in.-outer-diameter glass reactor tube. A plasma is generated in the reactor tube by the application of 50 W radio frequency power at 13.56 MHz through a pair of copper ring electrodes, coupled through an impedance matching network. The Ar and H_2 flow rates in the primary gas feed are fixed throughout this study at 25 and 20 sccm, respectively. H_2 is included in the primary gas feed in order to scavenge Cl resulting from the decomposition of $GeCl_4$.[25] The $GeCl_4$ precursor was selected as the Ge source over GeH_4 because of its lower toxicity and easier handling in laboratory conditions. The partial pressure of $GeCl_4$ was fixed throughout the study at 50 mTorr and 2.5% of the total pressure.

Si Shell Growth. Downstream of the Ge core growth region, an additional precursor is added through a second inlet to initiate shell growth. This secondary gas feed, composed of 5% silane diluted in Ar (5% SiH_4/Ar) and an additional feed of dilution Ar, is added to the plasma below the electrodes, a location that is sometimes referred to as the plasma afterglow. This secondary gas feed is injected into the coating region through a stainless steel vacuum fitting with 16 individual 1-mm-diameter holes spaced evenly around the circumference of the reactor. The vacuum fitting itself is grounded and serves as a counter electrode.

To control the shell thickness, 5% SiH_4/Ar was varied over a flow rate of 0−10 sccm, while the dilution Ar was carefully adjusted in opposition to maintain a constant total pressure of 2 Torr in the reactor. In this way, the concentration of silane in this feed can be varied from 0 to 5%. For example, thin Si shells are grown on the Ge core when the SiH_4 concentration in the secondary gas feed is 1%, while thick Si shells are grown when the SiH_4 concentration in the gas feed is 5%.

The presumed growth mechanism is that Ge nanoparticle nucleation and growth occurs in a diffuse, low-density plasma above the ring electrodes.[22] In this phase, as the particles grow predominantly by coagulation of initial clusters and "protoparticles", the particle concentration eventually drops below the positive-ion density, and the nanoparticles acquire, on average, at least one negative elementary charge per particle.[26] Importantly, this unipolar negative charging of the nanoparticles in the nonthermal plasma suppresses further particle coagulation, serving the role of organic surfactants in

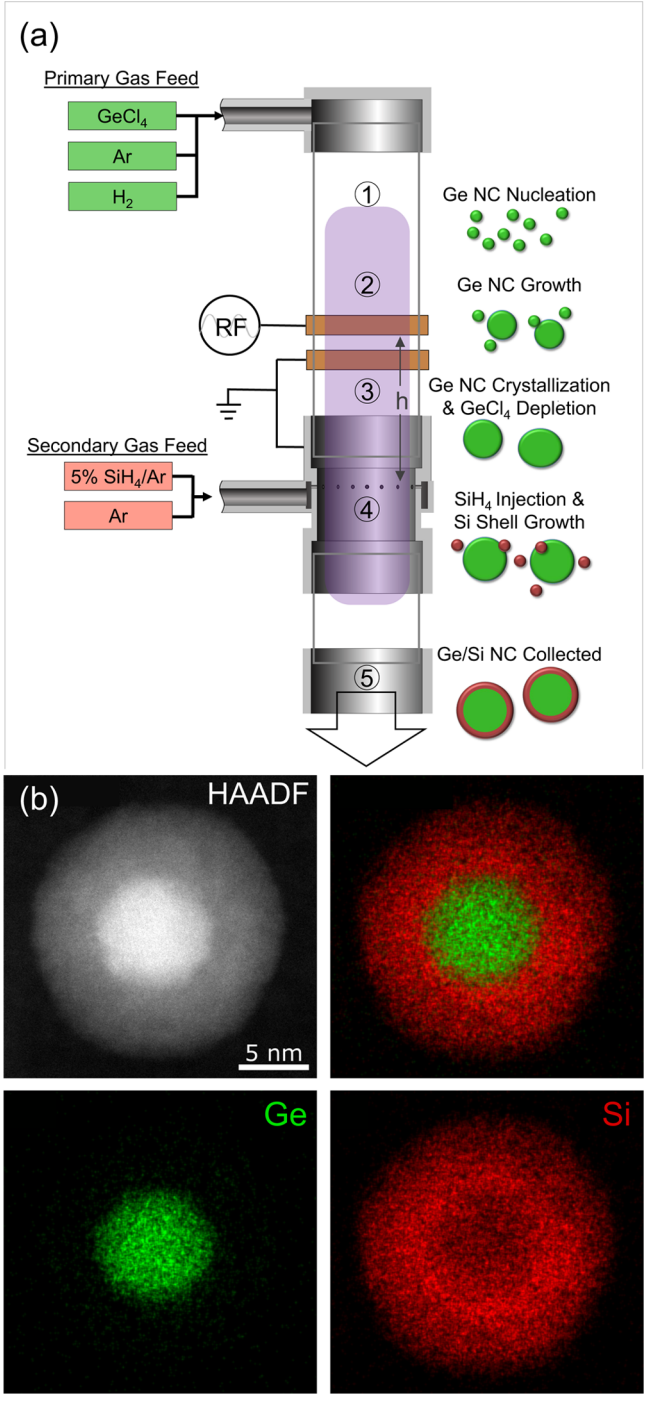

Figure 1. (a) Schematic of the flow-through nonthermal plasma reactor used for the synthesis of core/shell semiconductor QDs. Numbers 1−5 on the diagram indicate the stages of core/shell QD growth. (1) Electron-impact-initiated dissociation of a $GeCl_4$ precursor and subsequent particle nucleation.[22] (2) Ge QD growth dominated by agglomeration until the particle concentration falls below the positive-ion density of the plasma. (3) Ge QD growth by surface deposition of radical species and QD crystallization by energetic surface reactions.[23] (4) Silane injection, decomposition, and heterogeneous surface growth onto Ge QD cores. (5) Ge/Si core/shell QDs that exit the plasma reactor and are collected from the gas phase via impaction onto the substrate. (b) Select HAADF-STEM images of a single Ge/Si core/shell QD. The HAADF image shows a bright Ge core (Z = 32) surrounded by a Si shell (Z = 14). STEM−EDX elemental maps of Ge (green) and Si (red) show elemental segregation to the core and shell, respectively, as viewed in the

DOI: 10.1021/acsami.6b16170
ACS Appl. Mater. Interfaces 2017, 9, 8263−8270

Figure 1. continued

projection. A three-pixel Gaussian blur was applied to the EDX data to aid in visualization.

colloidal core/shell QD synthesis to keep nanoparticle cores separated. In the bright, higher-density discharge below the ring electrodes, the nanoparticles are heated above their crystallization temperature by energetic surface reactions.[23] In this region, the Ge precursor is depleted. Finally, the Si precursor is added to the plasma downstream of the Ge core growth region, initiating epitaxial gas-phase surface growth of a Si shell. Below this coating region, the QDs are accelerated through an orifice and impacted onto select substrates depending on the desired sample characterization. Samples are kept air-free by transfer through a load-lock system to a nitrogen (N_2)-purged glovebox.

Sample Characterization. To investigate their structure, core/shell QDs were deposited directly onto ultrathin/holey double C on Cu TEM grids and transferred with less than 30 s of air exposure into an aberration-corrected FEI Titan G2 60-300 (scanning) transmission electron microscope equipped with a Super-X energy-dispersive X-ray (EDX) device. STEM images were taken at 60 kV with a 25 mrad convergence semiangle and a 120 pA beam current. High-angle annular-dark-field scanning transmission electron microscopy (HAADF-STEM) images of QDs were acquired with 2048 × 2048 pixels over 240 × 240 nm for QD size distribution analysis. Spatially resolved STEM−EDX maps were collected with 740 × 740 pixels over 45 × 45 and 22 × 22 nm areas for single particles, with a dwell time of 4 μs/pixel, acquisition times of 10 min, and drift correction after every frame. The Si K and Ge K edges were background-subtracted and integrated, producing spectral images. A three-pixel Gaussian blur was applied to the final spectral images to reduce noise and aid in visualization. During acquisition, no visible damage to the QDs was observed. To assess the surface coverage of the core/shell QDs, QD films were deposited onto Al-coated silicon wafers and investigated by reflectance Fourier transform infrared (FTIR) spectroscopy in an oxygen-free, dry N_2-purged glovebox. To analyze the elemental composition of the core/shell QDs, films of Ge/Si QDs were deposited directly onto an Al-coated Si wafer and examined by SEM−EDX using a Jeol 6500 scanning electron microscope. The crystallinity and strain in the Ge/Si QDs deposited onto glass substrates was studied by X-ray diffraction (XRD) measurements. Diffraction patterns were collected on a Bruker D8 Discover diffractometer with a beryllium 2D area detector using a Co Kα source and were mathematically converted to Cu Kα patterns. For comparison, reference QDs composed of only Si were synthesized from $SiCl_4$ (2 sccm) in an Ar (25 sccm)−H_2 (20 sccm) plasma with no secondary gas feed and analyzed by identical means.

RESULTS

Ge/Si core/shell QDs were synthesized with increasing Si shell thickness, while the Ge core size was held constant by fixing the primary gas feed conditions, total flow rate, and pressure. The core/shell structure of these QDs is readily observed through HAADF-STEM, with the elemental distribution revealed by STEM−EDX mapping. Figure 1b shows a single spherical Ge core uniformly coated in a conformal Si shell. From this single particle, we see that the STEM−EDX elemental map accurately reflects the dimensions of both the core and shell as measured from the HAADF-STEM image. Visualization of each element shows the segregation of Ge to the core and Si to the shell. Because of the important impacts that the interface quality and composition have on the material properties, a detailed analysis of these STEM−EDX maps to determine the extent of Ge/Si segregation is currently under invegstigation and will be published in a forthcoming work.

Shell Coverage. Complete encapsulation of the Ge QD core by Si is confirmed by diffuse-reflectance FTIR spectroscopy. The FTIR signature is dominated by a surface bond with H and Cl species, residuals from precursor gases. Signatures of Ge, Ge/Si, and Si QD samples (Figure 2) reveal an ability to

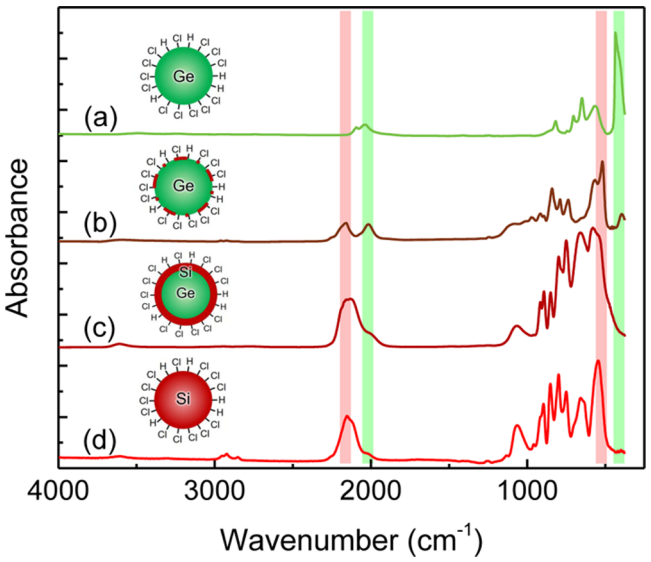

Figure 2. Diffuse-reflectance FTIR spectra of H- and Cl-terminated species: (a) Ge QDs; (b) Ge/Si QDs with partial shells; (c) Ge/Si QDs with complete shells; (d) Si QDs. Ge−Cl (425 cm^{-1}) and Ge−H (2000 cm^{-1}) absorption features are indicated with green vertical lines. Si−Cl (525 cm^{-1}) and Si−H (2150 cm^{-1}) absorption features are indicated with red vertical lines. Spectrum c of Ge/Si core/shell QDs is indistinguishable from spectrum d of Si QDs with Cl and Ge termination, indicating that the Ge core is fully encapsulated.

control the extent of shell coating from negligible to complete coverage of the Ge surface with Si. The absorption spectrum (a) of the uncoated Ge QDs exhibits a dominant feature around 425 cm^{-1}, corresponding to the stretching mode of Ge−Cl_x surface bonds, while a small, broad peak at 2000 cm^{-1} is attributable to the stretching mode of Ge−H_x surface bonds.[24] For comparison, the spectrum in Figure 2d was collected from Si QDs synthesized under identical nonthermal plasma conditions from $SiCl_4$. In this spectrum, the Si−Cl_x and Si−H_x stretching features are shifted to 525 and 2150 cm^{-1}, respectively. The spectrum in Figure 2c presents a representative absorption spectrum of the Ge/Si QDs, whose features are indistinguishable from those of the Si QDs from $SiCl_4$. The absence of Ge−Cl and Ge−H modes from this spectrum provides evidence of complete Si shell coverage of the Ge core. In contrast, an example of incomplete shell growth is shown in the spectrum in Figure 2b; Ge−Cl and Ge−H modes are still detectable. This sample was produced by increasing the separation of the electrode from the SiH_4 injection point to 10 cm such that the plasma density in the shell growth region was significantly suppressed and insufficient for complete coating of the Ge core.

Shell Thickness. The sample size dispersity of the Si/Ge core/shell particles is of particular interest for their optical properties. QDs produced from nonthermal plasmas, particularly Si QDs, have garnered much attention thanks to their narrow size distributions, which yield highly uniform optical properties. We find that, with growth of a Si shell on Ge QD cores, the size distribution remains monodisperse but broadens

DOI: 10.1021/acsami.6b16170
ACS Appl. Mater. Interfaces 2017, 9, 8263−8270

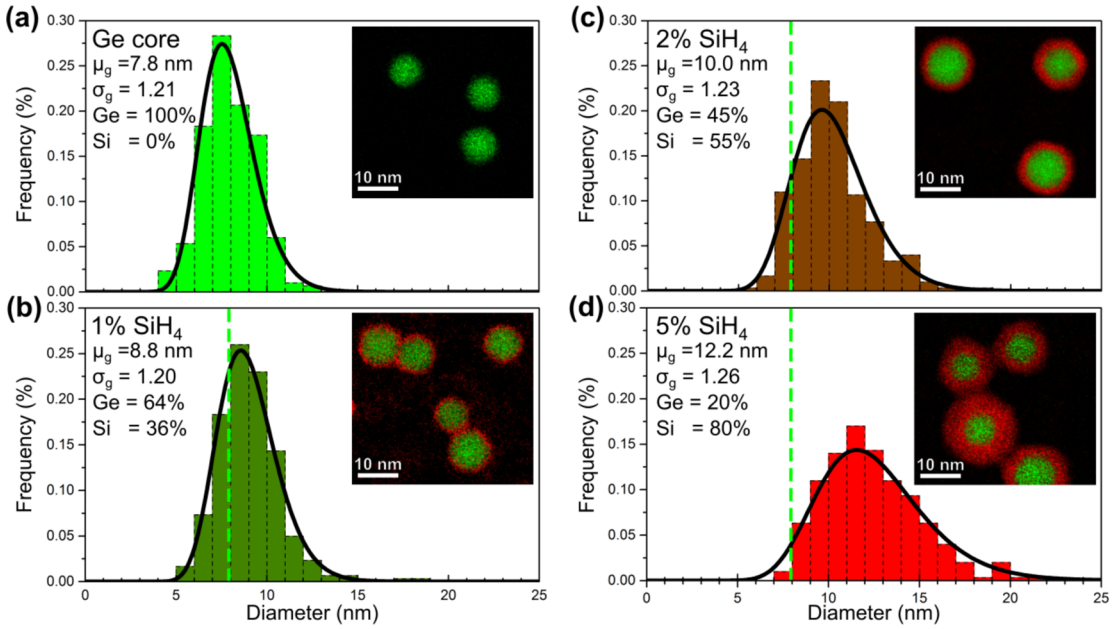

Figure 3. (a–d) Size distributions and representative STEM–EDX maps (inset) of Ge (green)/Si (red) core/shell QDs synthesized with 0, 1, 2, and 5% concentrations of SiH_4 in the secondary gas feed, respectively. The size distributions for each sample were determined from the measurement of the outer diameter of 300 QDs per sample. The geometric mean and standard deviation are estimated by fitting a histogram with a log-normal distribution. The dashed green lines on parts b–d denote the geometric means of Ge core distribution, as estimated from part a. Ensemble-average Ge and Si atomic percents for each sample were estimated from SEM–EDS elemental analysis (see the Supporting Information, section S1).

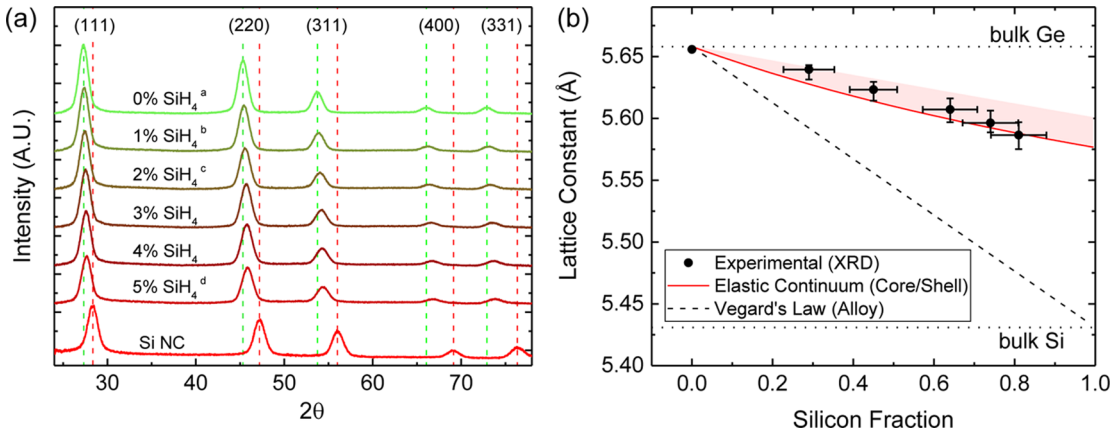

Figure 4. (a) Raw diffraction pattern for Ge/Si QDs with increasing Si shell thickness (top to bottom) synthesized with increasing concentration of SiH_4 in a secondary gas feed (0–5%). The diffraction peaks of uncoated Ge QDs closely match the bulk values (denoted with vertical dashed lines). With increasing Si shell thickness, the diffraction peaks broaden and shift to larger 2θ values. Diffraction patterns labeled a–d correspond to samples represented in Figure 3a–d. (b) Lattice constant (determined from XRD) versus Si fraction (determined from SEM–EDS). The dashed black line indicates the lattice constant of SiGe alloy QDs for a given Si fraction. The solid line indicates the lattice constant of a Ge/Si core/shell QD with a 8 nm Ge core for a given Si fraction using the continuum elasticity model.[27] The shaded region shows the range of lattice constants accessible for a Si elastic modulus between 50% and 100% of its bulk value, to account for softening of the shell at the nanoscale.

with increasing shell growth. Parts a–d in Figure 3 show images of QDs and their size distributions synthesized with the SiH_4 concentrations in the secondary feed at 0, 1, 2, and 5%, respectively. For each sample, the diameter of 300 QDs was measured from the HAADF-STEM images to determine the QD size distribution for each SiH_4 flow rate (see the Supporting Information, section S1). These QD sizes were fit to a log-normal distribution, and the fit parameters are summarized in Figure 3. With no SiH_4 in the secondary gas feed, uncoated Ge QDs are collected, and from these samples, we can determine a baseline size dispersity of σ_g = 1.21, characteristic of this nonthermal plasma synthesis approach.[10] With increasing SiH_4 in the secondary gas feed, the mean diameter of the QDs increases, indicative of controlled shell growth. The size distribution also broadens with increasing shell thickness because of a growing dispersity in the shell thickness with increasing SiH_4 feed rate. For comparison, the ensemble-average elemental composition of the Ge/Si core/shell at each shell thickness was determined by SEM–energy-dispersive spectroscopy (EDS) analysis of QD films (see the Supporting Information, section S2). The shell thickness estimated from this elemental analysis corroborates the increasing shell thickness estimates from the shift in the measured size distribution. This demonstrated ability to grow a wide range of shell thicknesses with minimal effect on the size

DOI: 10.1021/acsami.6b16170
ACS Appl. Mater. Interfaces 2017, 9, 8263–8270

distribution is important for preserving the ensemble optical performance.

Ge/Si Strain. The strain on the Ge cores caused by the 4% lattice mismatch with the Si shell is of particular interest because it has previously not been studied. Ge/Si core/shell QDs with increasing Si shell thickness were examined by XRD. Figure 4a displays the raw XRD data for Ge/Si core/shell QDs synthesized with an increasing percentage of SiH_4 in the secondary gas feed. Bulk Ge (green) and Si (red) crystal planes are denoted with vertical dashed lines. For even the highest SiH_4 flow rates used in this work, the diffraction patterns are consistent with single-crystal coherent growth. Two trends are seen in these diffraction patterns with increasing SiH_4 feed rate: (1) diffraction peaks shift to larger 2θ values relative to bulk Ge, indicative of lattice contraction; (2) there is a 2θ-dependent broadening of the diffraction peaks.

For a single diffraction pattern, the lattice constant is determined by taking the average of the five indexed diffraction planes, weighted by the quality of fit of a pseudo-Voigt profile using the MDI *Jade* software. The largest source of error in this lattice constant estimate is the sample-to-sample variation incurred during synthesis. For each synthesis condition, diffraction patterns are collected for three distinct samples. The average lattice constant of these three samples is shown in Figure 4b. Error bars indicate the range of lattice constants measured for each synthesis condition.

The lattice contraction of the QD ensemble with increasing SiH_4 feed rate can be explained by the addition of Si atoms (a_{Si} = 5.431 Å) to the large Ge QD lattice (a_{Ge} = 5.685 Å). If Ge and Si atoms form an alloy, the measured lattice constant will vary linearly with the atomic composition, as indicated by the dashed line in Figure 4b. Alternatively, if Si forms a shell around the Ge QD core, the compressive strain induced by the 4% lattice mismatch can be estimated by modeling each component as a bulk elastic continuum (see the Supporting Information, section S3).[27] The resulting lattice constant estimated from the continuum elasticity model for the Ge/Si core/shell system is given by the solid red line in Figure 4b, well matched by the experimentally determined lattice constants from XRD.

This continuum elasticity model has previously been used for comparison of the strain in core/shell NCs, for example, in CdTe/ZnSe.[6] It is important to note that the material properties of nanoparticles can vary significantly from the bulk values. However, because there are no generically applicable trends for the effect of the size on the elastic properties nor are there repeatedly documented measurements of these properties for our material size and geometry of interest, the bulk values have been used for these estimates. One likely deviation of the material properties from the bulk values is the possible softening of the Si shell for small shell thicknesses.[28] To further investigate the effects of this shell softening, the elastic continuum model was exercised with the elastic modulus of Si at 50% of bulk. The shaded region in Figure 4b represents the range of lattice constants accessible for a given Si fraction for an Si elastic modulus in the range of 50% to 100% of bulk. This softening would be particularly significant for the smallest Si fraction, having the thinnest shells.

0D and 1D nanostructures are known to be more accommodating of the strain than their 2D planar counterparts because of the large radius of curvature and the ability of both the substrate (core) and growth layer (shell) to accept strain, resulting in a larger critical thickness for the onset of defect formation. By comparing the elastic potential energy induced by strain to the energy required for defect formation, Balasubramanian et al.[27] estimated the critical shell thickness of the Ge/Si QD system. They found that a Ge QD core smaller than 10 nm can support a Si shell of any thickness without defect formation, consistent with coherent growth indicated by the diffraction patterns in this work. The broadening of the diffraction peaks in this work with increased Si content (Figure 4a) can be attributed to a dispersity in the strain resulting for the shell thickness dispersity, in agreement with the size distributions observed in STEM.

Ge/Si Optical Properties. The ability to control the optical properties with QD dimensions is key to the application of QDs in optoelectronic devices. Here, the affect of Si shell growth on the Ge QD band structure was interrogated through extinction measurements of Ge/Si QD films on glass substrates. Bulk Ge exhibits an indirect Γ−L transition of 0.67 eV followed by strong absorption onset at 0.80 eV from the direct Γ transition. This direct feature is easily observed experimentally as a steep rise and shoulder in the near-IR extinction spectrum of the Ge QD cores around 1200 nm (~1 eV), which is blue-shifted from the bulk E_0 transition shoulder due to quantum confinement.[29] With increasing Si shell thickness, the onset of direct absorption in the extinction spectra of the Ge/Si QDs blue shifts, indicative of a higher energy transition from heavy holes in the valence band to the Γ point in the conduction band (Figure 5a).

The energy of the first direct transition in the Ge core, from the heavy hole valence-band maximum at Γ to the conduction-band minimum at Γ ($E_{HH-c\Gamma}$), is estimated from where the first derivative of the extinction spectrum is maximized (Figure 5b), ignoring the weak, phonon-assisted band-gap transition, which manifests as a low-energy foot. The first direct transition feature blue shifts and broadens. The widening of the HH−cΓ transition can be attributed to strain-induced modulation of the Ge band structure with increasing Si shell thickness. The broadening of this feature is indicative of the increasing strain dispersity with increasing Si fraction, as observed in STEM size measurements and XRD measurements. For samples synthesized at the highest SiH_4 feed rates, the polydispersity of the size and strain in these samples blur out the transition, making it impossible to confidently determine the transition energy.

The variation of $E_{HH-c\Gamma}$ induced by compressive strain on the Ge core is plotted in Figure 5c, assuming that the change in the lattice constant observed in XRD is due entirely to strain. The offset in the transition energy of the unstrained Ge QDs is attributed to quantum confined band widening (E_{QC}). While this measurement cannot elucidate the effect of strain on the conduction and valence bands independently, a linear fit to the data estimates the combined deformation potential of the valence (a_v) and conduction (a_c) bands. Deformation potential theory describes how the allowed energy bands in a solid are perturbed by strain. The deformation potentials of the valence and conduction bands in bulk Ge have been of increasing interest based on the promise of using strain to induce a direct transition in this normally indirect-band-gap material.[31] We have followed the framework presented in ref 30 to estimate Ge band deformation with strain (see the Supporting Information, section S4).

The relavent effects on the energy of the first direct transition are summarized in eq 1.

$$E_{HH-c\Gamma} = E^{(0)}_{HH-c\Gamma} + E_{QC} + (a_c - a_v) \times 3(-\epsilon) \quad (1)$$

DOI: 10.1021/acsami.6b16170
ACS Appl. Mater. Interfaces 2017, 9, 8263−8270

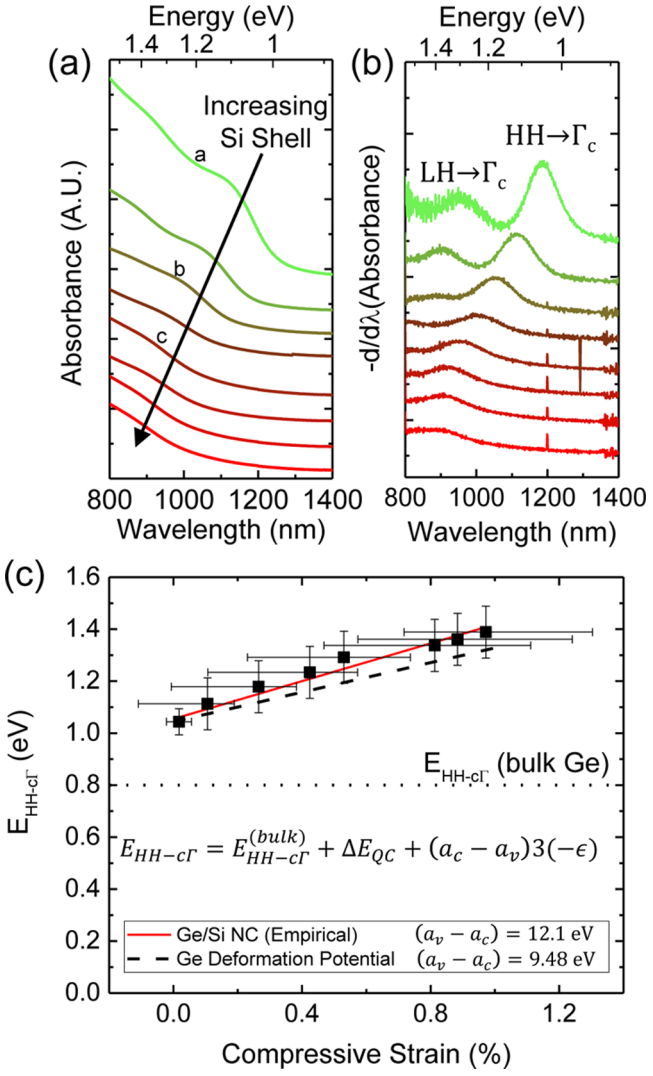

Figure 5. (a) Raw near-IR extinction spectra for Ge/Si QDs with increasing Si shell thickness (top to bottom). Spectra are offset for clarity. (b) Derivatives of extinction spectra indicating blue shifts and broadening of the onset of direct absorption with increasing Si shell thickness (top to bottom). Spectra are offset for clarity. Spectra labeled a–c correspond to samples represented in Figure 3a–c. (c) Energy of the heavy hole to conduction band Γ-point transition ($E_{HH-c\Gamma}$) modulated with strain. For each Ge/Si sample, the compressive strain was determined from the shift in the XRD peak positions relative to Ge, while $E_{HH-c\Gamma}$ was estimated by finding the peak in part b. A linear fit to the experimental data (red) was used to estimate the combination of valence- and conduction-band deformation potentials ($a_v - a_c$), compared to the published values[30] for the deformation potential values of Ge (dashed line).

The three terms on the right-hand side of the equation can be explained as follows: (1) the first term is the energy of the HH−cΓ transition in bulk Ge, 0.8 eV; (2) the second term is the widening of the band gap due to quantum confinement, with $1/R_{NC}^2$ dependence, taken as a constant for a single Ge NC core size distribution; (3) the third term is the combined effect of hydrostatic compressive strain (ϵ) on the deformation of the valence and conduction bands. The data in Figure 5c are fit to this equation such that the slope of the fit is $-(a_c - a_v)$.

Experimental and theoretical estimates of the values for these deformation potentials are widely available in the literature[30] because of recent interest in the transition to a direct band gap in tensile-strained Ge;[31] these values are used to estimate a predicted blue shift in $E_{HH-c\Gamma}$ with strain (dashed line in Figure 5c) compared to the measured value (solid red line in Figure 5c).

DISCUSSION

The synthesis approach introduced here enables delicate control over the shell thickness via four parameters that affect the shell growth region of the plasma: (1) SiH_4 axial concentration profile, $n_{SiH_4}(z)$, set by the SiH_4 concentration in the secondary gas feed; (2) plasma electron density axial profile, $n_e(z)$, in the coating region set by the input power and electrode height, h; (3) core Ge QD size, $d_{Ge\ QD}$, and concentration, $n_{Ge\ QD}$, set by the primary gas feed conditions, which provide an effective surface area flux through the coating region; (4) QD residence time within the coating region, set by the total gas flow rate and pressure. Effectively, these experimental conditions dictate the number of collisions between a QD core and silyl radicals during transition to the shell growth region. In this work, the shell thickness was modulated using only variations in the shell precursor (SiH_4) concentration, while all other factors were carefully controlled. The plasma density profile in the shell growth region was held constant by the consistently applying 50 W of radio-frequency power and holding the powered electrode height at a fixed 6 cm distance away from the point of shell precursor injection. The Ge QD core size and concentration were fixed by holding the primary gas feed rates constant. The QD residence time was fixed by keeping the total gas flow fixed at 55 sccm and the pressure fixed at 2 Torr.

Experimentally, no Si-only QDs are observed in STEM. This indicates that heterogeneous surface growth is dominant over the homogeneous nucleation of silyl clusters and subsequent Si QD growth. For heterogeneous surface growth to be preferred over Si nucleation, the concentration of silyl radicals must remain below a nucleation threshold, which is maintained provided that the rate of radical consumption by heterogeneous surface growth is faster than the rate of radical generation by dissociative reactions.

CONCLUSION

In conclusion, we have demonstrated that nonthermal plasmas provide a unique reaction environment, well-suited to the gas-phase growth of core/shell QDs. Specifically, the negative charging of core QDs in the plasma suppresses coagulation, keeping the QDs singly dispersed, such that shell growth occurs around isolated particles rather than agglomerates. Effectively, Coulombic repulsion between QDs provides a barrier to core agglomeration generally afforded by organic surfactants in solution-phase approaches. Additionally, the in-flight selective heating of these QDs exploits the nonequilibrium within the plasma such that $T_{gas} < T_{QD} < T_e$. This allows for the synthesis of materials requiring high synthesis temperatures, while the background gas is maintained near room temperature.[23] Finally, a low plasma density in the shell growth region limits the generation rate of silyl radicals, favoring heterogeneous shell growth over homogeneous nucleation of shell particles.

This gas-phase approach to the core/shell QD synthesis is particularly indiscriminate of the desired material, unlike colloidal growth, which requires careful optimization of growth conditions and ligand selection. Nonthermal plasmas have been used for the synthesis of Si (P- and B-doped),[7] Ge,[25] SiGe,[32]

DOI: 10.1021/acsami.6b16170
ACS Appl. Mater. Interfaces 2017, 9, 8263–8270

ZnO (Al-doped),[33] ZnS,[34] GaN,[35] and InP,[36] to name a few. The methods presented here should allow for the synthesis of novel, technologically relevant core/shell QDs, which have so far been difficult or impossible to produce in solution.

■ ASSOCIATED CONTENT

Supporting Information

The Supporting Information is available free of charge on the ACS Publications website at DOI: 10.1021/acsami.6b16170.

Representative HAADF-STEM images, SEM−EDS spectra and atomic composition (Ge/Si), continuum elasticity model details and calculation of the lattice strain, and deformation potential theory estimates of Ge band modulation from strain (PDF)

■ AUTHOR INFORMATION

Corresponding Authors

*E-mail: hunte454@umn.edu.

*E-mail: kortshagen@umn.edu.

ORCID

Katharine I. Hunter: 0000-0001-8639-5012

Notes

The authors declare no competing financial interest.

■ ACKNOWLEDGMENTS

This work was supported primarily by the U.S. National Science Foundation (NSF) through the University of Minnesota MRSEC under Award DMR-1420013. K.I.H. acknowledges support by the NSF Graduate Research Fellowship Program under Grant 00039202. U.R.K. was supported by the U.S. Department of Energy (DOE), Center for Advanced Solar Photophysics, an Energy Frontier Research Center funded by the U.S. DOE, Office of Science, Basic Energy Sciences. Parts of this work were carried out in the Characterization Facility, University of Minnesota, which receives partial support from the NSF through the MRSEC program.

■ REFERENCES

(1) Murray, C. B.; Norris, D.; Bawendi, M. G. Synthesis and Characterization of Nearly Monodisperse CdE (E= S, Se, Te) Semiconductor Nanocrystallites. *J. Am. Chem. Soc.* **1993**, *115*, 8706−8715.

(2) Dabbousi, B. O.; Rodriguez-Viejo, J.; Mikulec, F. V.; Heine, J. R.; Mattoussi, H.; Ober, R.; Jensen, K. F.; Bawendi, M. G. (CdSe)ZnS Core - Shell Quantum Dots: Synthesis and Characterization of a Size Series of Highly Luminescent Nanocrystallites. *J. Phys. Chem. B* **1997**, *101*, 9463−9475.

(3) Li, J. J.; Wang, Y. A.; Guo, W.; Keay, J. C.; Mishima, T. D.; Johnson, M. B.; Peng, X. Large-scale Synthesis of Nearly Monodisperse CdSe/CdS Core/Shell Nanocrystals using Air-stable Reagents via Successive Ion Layer Adsorption and Reaction. *J. Am. Chem. Soc.* **2003**, *125*, 12567−12575.

(4) Kim, S.; Fisher, B.; Eisler, H. J.; Bawendi, M. Type-II Quantum Dots: CdTe/CdSe(core/shell) and CdSe/ZnTe(core/shell) Heterostructures. *J. Am. Chem. Soc.* **2003**, *125*, 11466−11467.

(5) Eychmuller, A.; Mews, A.; Weller, H. A Quantum Dot Quantum Well: CdS/HgS/CdS. *Chem. Phys. Lett.* **1993**, *208*, 59−62.

(6) Smith, A. M.; Mohs, A. M.; Nie, S. Tuning the Optical and Electronic Properties of Colloidal Nanocrystals by Lattice Strain. *Nat. Nanotechnol.* **2009**, *4*, 56−63.

(7) Pi, X. D.; Gresback, R.; Liptak, R. W.; Campbell, S. A.; Kortshagen, U. Doping Efficiency, Dopant Location, and Oxidation of Si Nanocrystals. *Appl. Phys. Lett.* **2008**, *92*, 123102.

(8) Alam, M. K.; Flagan, R. C. Controlled Nucleation Aerosol Reactors: Production of Bulk Silicon. *Aerosol Sci. Technol.* **1986**, *5*, 237−248.

(9) Littau, K. A.; Szajowski, P. J.; Muller, A. J.; Kortan, A. R.; Brus, L. E. A Luminescent Silicon Nanocrystal Colloid via a High-Temperature Aerosol Reaction. *J. Phys. Chem.* **1993**, *97*, 1224−1230.

(10) Mangolini, L.; Thimsen, E.; Kortshagen, U. High-yield Plasma Synthesis of Luminescent Silicon Nanocrystals. *Nano Lett.* **2005**, *5*, 655−659.

(11) De Oliveira, E. L.; Albuquerque, E. L.; De Sousa, J. S.; Farias, G. a.; Peeters, F. M. Configuration-Interaction Excitonic Absorption in Small Si/Ge and Ge/Si core/shell Nanocrystals. *J. Phys. Chem. C* **2012**, *116*, 4399−4407.

(12) Nestoklon, M. O.; Poddubny, A. N.; Voisin, P.; Dohnalova, K. Tuning Optical Properties of Ge Nanocrystals by Si Shell. *J. Phys. Chem. C* **2016**, *120*, 18901−18908.

(13) Xiang, J.; Lu, W.; Hu, Y.; Wu, Y.; Yan, H.; Lieber, C. M. Ge/Si Nanowire Heterostructures as High-Performance Field-Effect Transistors. *Nature* **2006**, *441*, 489−493.

(14) Xiang, J.; Vidan, A.; Tinkham, M.; Westervelt, R. M.; Lieber, C. M. Ge/Si Nanowire Mesoscopic Josephson Junctions. *Nat. Nanotechnol.* **2006**, *1*, 208−213.

(15) Hu, Y.; Kuemmeth, F.; Lieber, C. M.; Marcus, C. M. Hole Spin Relaxation in Ge−Si Core−Shell Nanowire Qubits. *Nat. Nanotechnol.* **2011**, *7*, 47−50.

(16) Li, B.; Liu, J. Nonvolatile Memory With Ge/Si Heteronanocrystals. *IEEE Trans. Nanotechnol.* **2011**, *10*, 284−290.

(17) Tayagaki, T.; Hoshi, Y.; Usami, N. Investigation of the Open-Circuit Voltage in Solar Cells Doped with Quantum Dots. *Sci. Rep.* **2013**, *3*, 2703.

(18) Yamasaka, S.; Watanabe, K.; Sakane, S.; Takeuchi, S.; Sakai, A.; Sawano, K.; Nakamura, Y. Independent Sontrol of Electrical and Heat Conduction by Nanostructure Designing for Si-based Thermoelectric Materials. *Sci. Rep.* **2016**, *6*, 22838.

(19) Eshed, M.; Keinan-adamsky, K.; Goobes, G.; Gedanken, A. Preparation of Ge@Organosilicon Core-Shell Structures and Characterization by Solid State NMR and Other Techniques. *J. Phys. Chem. C* **2013**, *117*, 11086−11094.

(20) Yang, C.-S.; Kauzlarich, S. M.; Wang, Y. C. Synthesis and Characterization of Germanium/Si-Alkyl and Germanium/Silica Core-Shell Quantum Dots. *Chem. Mater.* **1999**, *11*, 3666−3670.

(21) Mehringer, C.; Kloner, C.; Butz, B.; Winter, B.; Spiecker, E.; Peukert, W. Germanium-Silicon Alloy and Core-Shell Nanocrystals by Gas Phase Synthesis. *Nanoscale* **2015**, *7*, 5186−5196.

(22) Bouchoule, A.; Boufendi, L. Particulate Formation and Dusty Plasma Behaviour in Argon-Silane RF Discharge. *Plasma Sources Sci. Technol.* **1993**, *2*, 204−213.

(23) Kramer, N. J.; Anthony, R. J.; Mamunuru, M.; Aydil, E. S.; Kortshagen, U. R. Plasma-induced Crystallization of Silicon Nanoparticles. *J. Phys. D: Appl. Phys.* **2014**, *47*, 075202.

(24) Cernetti, P.; Gresback, R.; Campbell, S. A.; Kortshagen, U. Nonthermal Plasma Synthesis of Faceted Germanium Nanocrystals. *Chem. Vap. Deposition* **2007**, *13*, 345−350.

(25) Gresback, R.; Holman, Z.; Kortshagen, U. Nonthermal Plasma Synthesis of Size-Controlled, Monodisperse, Freestanding Germanium Nanocrystals. *Appl. Phys. Lett.* **2007**, *91*, 093119.

(26) Kortshagen, U.; Bhandarkar, U. Modeling of Particulate Soagulation in Low Pressure Plasmas. *Phys. Rev. E: Stat. Phys., Plasmas, Fluids, Relat. Interdiscip. Top.* **1999**, *60*, 887−898.

(27) Balasubramanian, S.; Ceder, G.; Kolenbrander, K. D. Three-Dimensional Epitaxy: Thermodynamic Stability Range of Coherent Germanium Nanocrystallites in Silicon. *J. Appl. Phys.* **1996**, *79*, 4132.

(28) Sadeghian, H.; Yang, C. K.; Goosen, J. F. L.; van der Drift, E.; Bossche, A.; French, P. J.; van Keulen, F. Characterizing size-dependent effective elastic modulus of silicon nanocantilevers using electrostatic pull-in instability. *Appl. Phys. Lett.* **2009**, *94*, 221903.

(29) Holman, Z. C.; Kortshagen, U. R. Absolute Absorption Cross Sections of Ligand-Free Colloidal Germanium Nanocrystals. *Appl. Phys. Lett.* **2012**, *100*, 133108.

(30) Boztug, C.; Sanchez-Perez, J. R.; Cavallo, F.; Lagally, M. G.; Paiella, R. Strained-Germanium Nanostructures for Infrared Photonics. *ACS Nano* **2014**, *8*, 3136−3151.
(31) Liu, J.; Sun, X.; Pan, D.; Wang, X.; Kimerling, L. C.; Koch, T. L.; Michel, J. Tensile-strained, n-type Ge as a Gain Medium for Monolithic Laser Integration on Si. *Opt. Express* **2007**, *15*, 11272−11277.
(32) Pi, X. D.; Kortshagen, U. Nonthermal Plasma Synthesized Freestanding Silicon−Germanium Alloy Nanocrystals. *Nanotechnology* **2009**, *20*, 295602.
(33) Greenberg, B. L.; Ganguly, S.; Held, J. T.; Kramer, N. J.; Mkhoyan, K. A.; Aydil, E. S.; Kortshagen, U. R. Nonequilibrium-Plasma-Synthesized ZnO Nanocrystals with Plasmon Resonance Tunable via Al Doping and Quantum Confinement. *Nano Lett.* **2015**, *15*, 8162−8169.
(34) Thimsen, E.; Kortshagen, U. R.; Aydil, E. S. Nonthermal Plasma Synthesis of Metal Sulfide Nanocrystals from Metalorganic Vapor and Elemental Sulfur. *J. Phys. D: Appl. Phys.* **2015**, *48*, 314004.
(35) Anthony, R.; Thimsen, E.; Johnson, J.; Campbell, S.; Kortshagen, U. A Non-thermal Plasma Reactor for the Synthesis of Gallium Nitride Nanocrystals. *MRS Online Proc. Libr.* **2005**, *892*, 221−224.
(36) Gresback, R.; Hue, R.; Gladfelter, W. L.; Kortshagen, U. R. Combined Plasma Gas-Phase Synthesis and Colloidal Processing of InP/ZnS Core/Shell Nanocrystals. *Nanoscale Res. Lett.* **2011**, *6*, 68.

DOI: 10.1021/acsami.6b16170
ACS Appl. Mater. Interfaces 2017, 9, 8263−8270